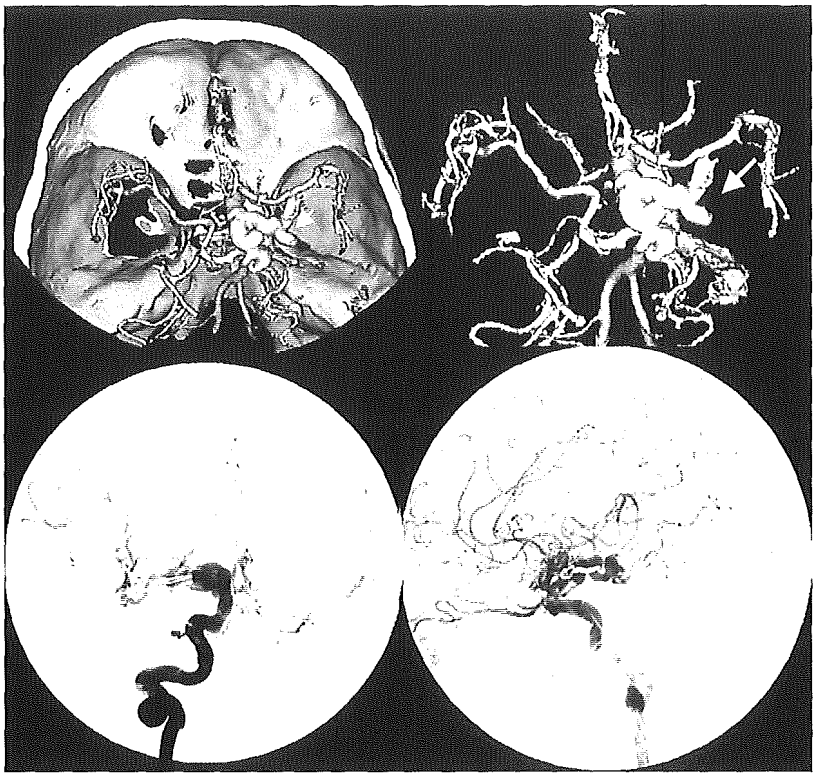

Fig. 2. Upper row: Three dimensional CT angiograms reveal a saccular aneurysm in the dolicho-ectatic right internal carotid artery. The aneurysm (arrow) was located in the crural cistern and extending into the inferior horn of the lateral ventricle. Lower row: The postoperative digital subtraction angiograms show the successful clipping of the aneurysm

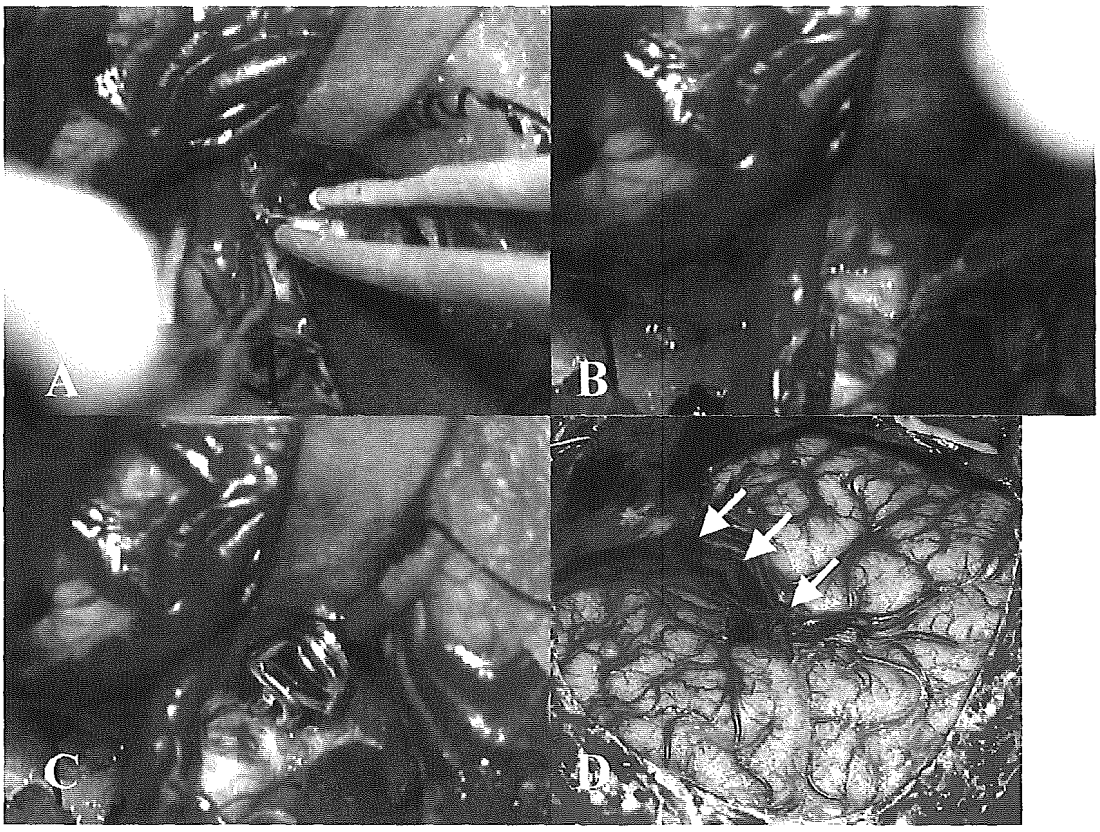

Fig. 3. Operative views of Case 1. (A): Splitting of the limen insula. (B): Neck dissection of aneurysm in the crural cistern. (C): Clipping of the aneurysm Neck. (D): Brain surface just after the clipping of the aneurysm showing the extent of the Sylvian fissure dissection (arrows)

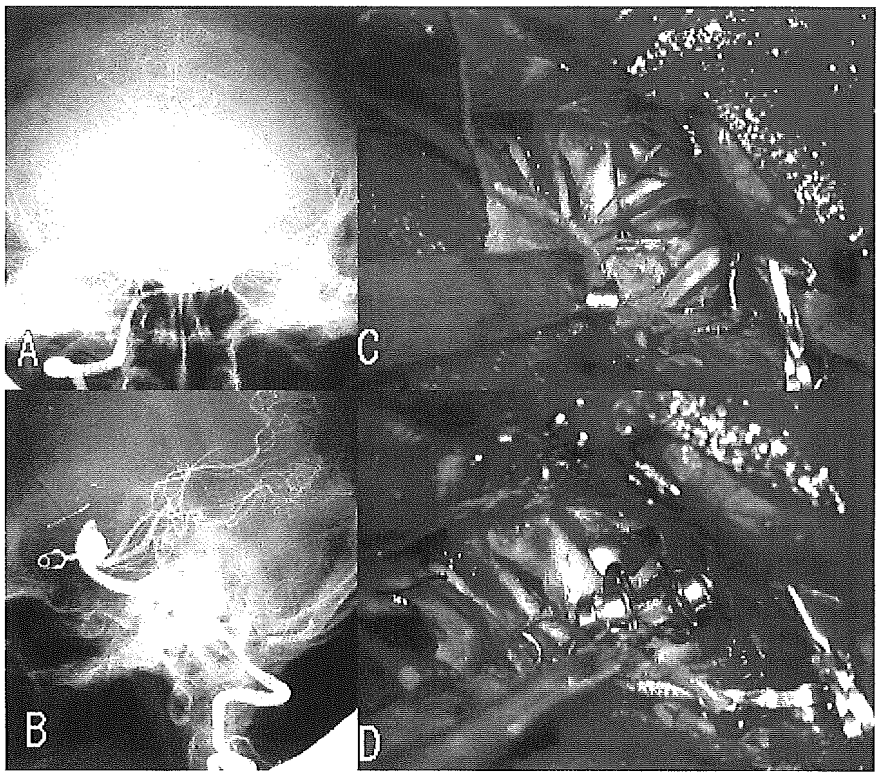

Fig. 4. Case 2: (A and B): The left vertebral angiograms reveal a large aneurysm at the origin of the right superior cerebellar artery. The aneurysm clip applied 20 years ago is observed at the tip of the dome of the aneurysm. (C): The operative view through the transsylvian trans-limen insular approach. The crural and ambient cisterns are widely exposed. The aneurysm was dissected free from the right posterior cerebral and superior cerebellar arteries. (D): With two fenestrated clips, the neck of the aneurysm was obliterated from the supero-lateral direction

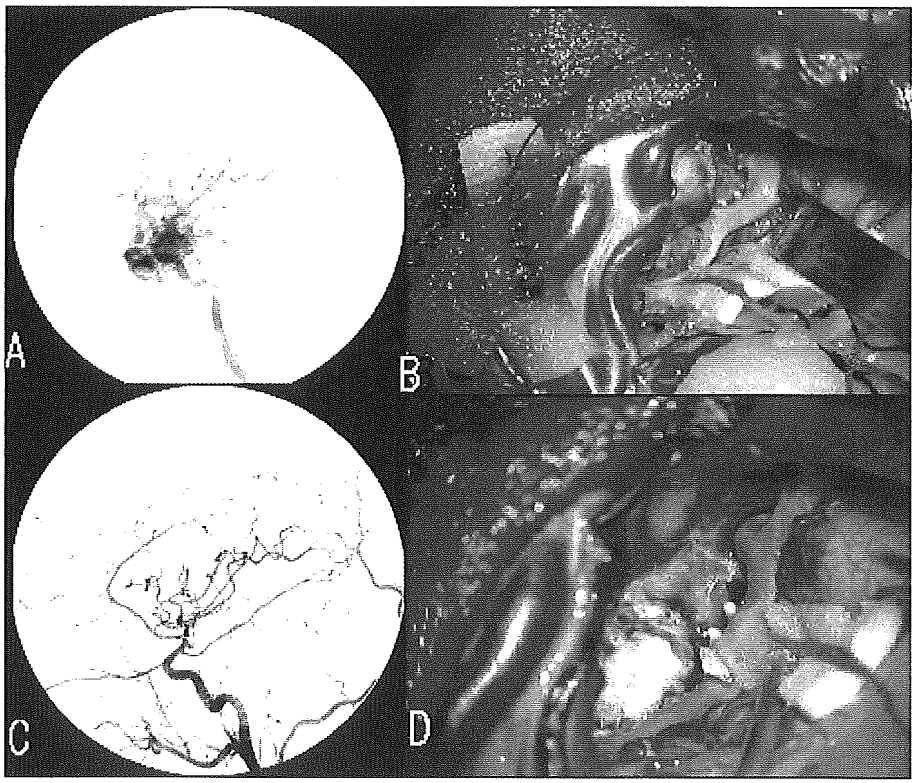

Fig. 5. Case 4: (A): The lateral view of the preoperative left carotid angiogram shows an arteriovenous malformation at the antero-medial temporal lobe. (B) The Sylvian fissure is widely opened and the feeding arteries from the middle cerebral artery and the anterior choroidal artery are exposed. (D) The nidus of the arteriovenous malformation located at the anterior temporal stem is totally removed. (C) The postoperative digital subtraction angiogram reveals the total removal of the nidus

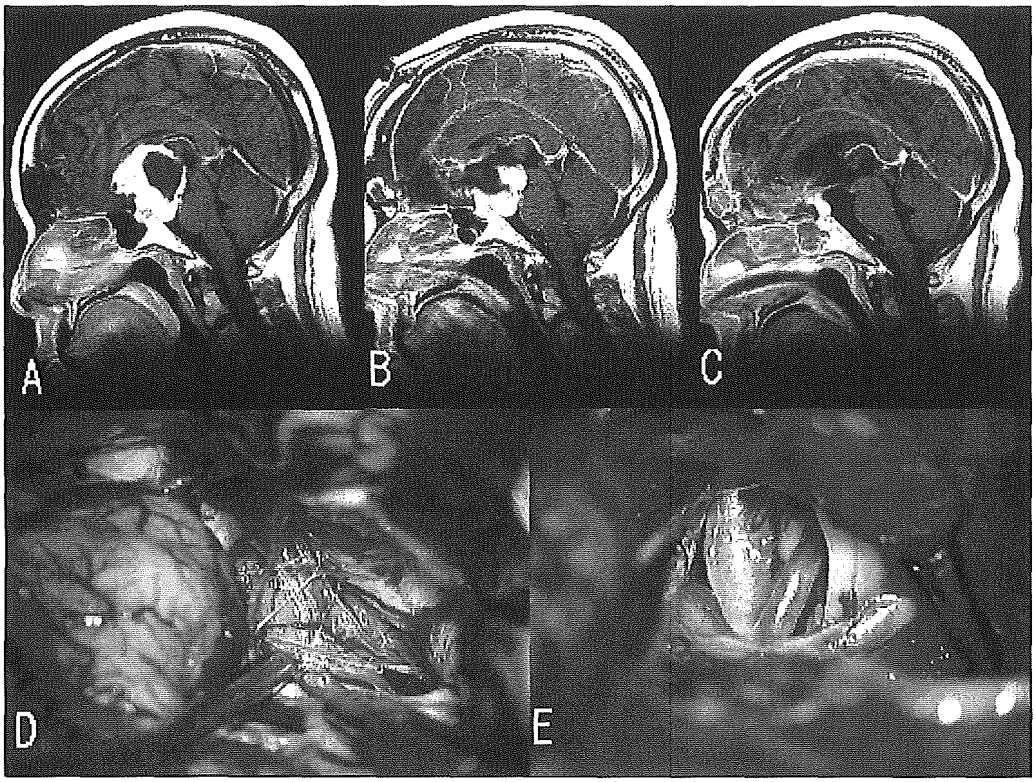

Fig. 6. Case 5: (A): A sagittal image of gadolinium enhanced MRI showed a large suprasellar craniopharyngioma. (B): At the first operation through the anterior interhemispheric approach, the antero-superior part of the tumor was removed. (C): At the second operation through the transsylvian trans-limen insular approach, the remnant tumor in the interpeduncular cistern was removed. (D): The operative view at the second operation. The tumor occupied the crural and ambient cisterns. Branches of the posterior communicating artery were identified on the tumor surface and were detached from the tumor. (E): The interpeduncular part of the tumor was removed and the basilar artery and the right superior cerebellar artery were exposed

In 2 patients with posterior fossa aneurysm (Cases 2 and 3), the neck clipping was successful under the good visualization of the basilar, posterior cerebral and superior cerebellar arteries. However, temporal lobe infarction was encountered in the patient with the superior cerebellar artery aneurysm after surgery. The preoperative deep drowsy conditions were not improved in either patient after surgery. A correct assessment of the neuropsychological consequences was not obtained. In the patient with the craniopharyngioma remnant (Case 5), the tumour in the interpeduncular cistern was well visualized through the widely opened crural and ambient cisterns. The tumour was carefully dissected from the arachnoid surface of the pons. The basilar artery and the branches were well identified and preserved at the tumour removal. The postoperative MRI showed the extirpation of the tumour extending to the interpeduncular cistern (Fig. 5). Because of the postoperative persistent confusion and drowsiness probably due to hypothalamic dysfunction, the correct assessment of the neuropsychological consequence was not obtained. There were no additional complications for patients with isolated inferior horn hydrocephalus (Cases 6 and 7) though the neuropsychological tests were not fully examined.

Discussion

The concept of the transsylvian trans-limen insular approach is a wide opening of the Sylvian cistern. This approach is intended to enter into the crural, the anterior part of the ambient and the superoposterior part of the interpeduncular cisterns. The microsurgical anatomy of this area has been reported as a transinsular transchoroidal approach by Ulm *et al.* [6]. Their concept of the approach is for the exposure of the posterior third of the crural, upper two-thirds of the ambient and the proximal quadrigeminal cisterns. Our approach is basically same as that described by Yasargil for the transsylvian selective amygdalohippocampectomy [10, 11], though it does not cut the temporal stem and we do not remove the amygdala. With regard to the exposure of the posterior cerebral artery, our approach is for the exposure of the

proximal P2 segment around the cerebral peduncle, instead of the distal P2 segment for the transinsular transchoroidal approach [8]. For the operation of the distal P2–P3 aneurysm, for example, we will not choose the transsylvian trans-limen insular approach, but the subtemporal approach. The most distinctive procedure of our approach is the splitting of the limen insula. The purpose of our approach is not to enter into deep and narrow regions through the choroidal fissure, but to widen the Sylvian cistern by splitting the limen insula.

The inferior limiting sulcus of the insular cortex is the closest region of entry into the inferior horn of the lateral ventricle as well as the collateral sulcus. There are many variations of the insular segment of the middle cerebral artery and the deep Sylvian vein [5–7]. A small branch of the deep Sylvian vein might be sacrificed in cutting the inferior limiting sulcus. The most appropriate region of the inferior limiting sulcus incision is generally 15 to 20 mm behind the limen insula. The preoperative MR images, particularly on coronal sections and the intraoperative neuronavigation system will be helpful to adjust the differences in individual cases. The shorter the incision of the inferior limiting sulcus, the better for preservation the temporal stem. A complete incision of the temporal stem results in severe deficits in learning and the ability to retain learned tasks [1, 3]. The incision of the inferior limiting sulcus posteriorly along the inferior horn of the lateral ventricle will result in severe neuropsychological deficits due to damage to the temporal stem. The posterior extension of the insular incision is not necessary for the transsylvian trans-limen insular approach.

The choroidal fissure in the inferior horn can be identified by retracting the choroid plexus superiorly. The anterior choroidal artery enters into the choroid plexus via the taenia choroidea on the mesencephalic side of the attachment. It is recommended to open the choroidal fissure in the taenia fimbriae between the choroid plexus and the fimbria to avoid the damage to the anterior choroidal artery [4]. In opening the choroidal fissure to the ambient cistern, care has to be taken not to damage the fragile vessels in the cistern, particularly in elderly patients. The choroidal fissure is opened anteriorly to the anterior end at the inferior choroidal point.

The limen insula is incised between the inferior choroidal point and the inferior limiting sulcus of the insular cortex. The uncinate fasciculus is incised at the limen insula. The fasciculus is the fiber connection between the orbitofrontal cortex and the temporal pole. Ebeling and Cramon [1] emphasized that even the damage of the anterior temporal stem might be responsible for various cognitive deficits. Patients who underwent selective amygdalohippocampectomy usually will not show neuropsychological complications [9]. There were no cognitive deficits among patients who underwent incision of the limen insula for aneurysm in the crural cistern and AVM in the medial temporal lobe. The cognitive deficits following temporal lobectomy are probably due to the interruption of fibre connections between the amygdala, temporal lobe and thalamus [2, 8]. Though the complications of the unilateral incision of the uncinate fasciculus are thought to be subclinical or transient, neuropsychological tests should be performed on all these patients, if possible, to prove the validity of the approach.

The wide exposure of the crural and ambient cisterns is the major advantage of the approach. However, the temporal branches of the middle cerebral artery and the superficial veins within the trajectory are exposed to the risk of damage. The temporal branches of the middle cerebral artery should be detached from the surface of the temporal lobe as much as possible to avoid damage from the retraction. In our cases, however, temporal lobe infarctions developed in two patients who underwent surgical manipulations in the interpeduncular cistern through the widely opened Sylvian cistern. Careful brain retraction and some other techniques will be necessary to avoid temporal lobe infarction, such as: 1. an even retraction of the frontal and temporal lobes, 2. an approach through the completely dissected middle cerebral artery in the Sylvian fissure or 3. EC-IC bypass to the temporal branch of the middle cerebral artery before entering into the interpeduncular cistern.

The transsylvian trans-limen insular approach is indicated for lesions in the crural and the anterior ambient cisterns, and lesions that need wider exposure of the interpeduncular cistern than the usual pterional exposure. For the former lesions, this approach can afford satisfactory results. For the latter lesions, we need to have further technical improvements and neuropsychological assessments.

References

1. Ebeling U, von Cramon D (1992) Topography of the uncinate fascicle and adjacent temporal fibre tracts. Acta Neurochir (Wien) 115: 143–148
2. Harding A, Halliday G, Caine D, Kril J (2000) Degeneration of anterior thalamic nuclei differenciates alcoholics with dementia. Brain 123: 141–154
3. Horel JA (1978) The neuroanatomy of amnesia. A critique of the hippocampal memory hypothesis. Brain 101: 403–445
4. Nagata S, Rhoton AL Jr, Barry M (1988) Microsurgical anatomy of the choroidal fissure. Surg Neurol 30: 3–59

5. Tanriover N, Rhoton AL Jr, Kawashima M, Ulm AJ, Yasuda A (2004) Microsurgical anatomy of the insula and the sylvian fissure. J Neurosurg 100: 891–922
6. Ulm AJ, Tanriover N, Kawashima M, Campero A, Bova FJ, Rhoton AL Jr (2004) Microsurgical approaches to the perimesencephalic cisterns and related segments of the posterior cerebral artery: comparison using a novel application of image guidance. Neurosurgery 54: 1313–1328
7. Varnavas GG, Grand W (1999) The insular cortex: morphological and vascular anatomic characteristics. Neurosurgery 44: 127–138
8. Visser PJ, Krabbendam L, Verhey FR, Hofman PA, Verhoeven WM, Tuinier S, Wester A, Den Berg YW, Goessens LF, Werf YD, Jolles J (1999) Brain correlates of memory dysfunction in alcoholic Korsakoff's syndrome. J Neurol Neurosurg Psychiatry 67: 774–778
9. Wieser HG (1986) Selective amygdalohippocampectomy: Indications, investigative technique and results. In: Symon L *et al* (eds) Advances and technical standards in neurosurgery, vol 13. Springer, Wien New York, pp 39–133
10. Yasargil MG (1996) Microneurosurgery, vol IVB. G. Thieme New York, pp 252–290
11. Yasargil MG, Teddy J, Roth P (1885) Selective amygdalohippocampectomy – operative anatomy and surgical technique. In: Symon L *et al* (eds) Advances and technical standards in neurosurgery, vol 12. Springer, Wien New York, pp 93–123

Comments

The concept of this approach is important and interesting. I have used the same approach in a number of cases in order to avoid damage by retraction. I never divide any of the temporal branches of MCA. The anatomy of these branches is quite variable and often it is possible to expose the limen in front of the anterior temporal artery. For a limited approach to the temporal horn the space between two arterial branches may suffice. In my opinion incision of the insula should be kept to a minimum. In most cases of the present series a minimal incision appears to have been used. And the results in these "moderate cases" were good. In some of the cases of the series, however, too much was done and temporal lobe infarction resulted. Therefore it is important to keep the potential risks of this approach in mind. When used carefully the concept of a translimen approach can certainly enlarge the horizon of the pterional transsylvian approach.

H.-J. Steiger
Düsseldorf

When accessing the perimesencephalic cisterns, the main advantage of an incision in the anterior temporal stem at the inferior limiting sulcus of the insula is to transchoroidally reach the posterior crural and ambient cisterns, especially in their more superior aspects. The standard pterional transsylvian approach does not allow a view of the ambient cistern due to the cerebral peduncle. However this approach does allow an excellent view of the interpeduncular cistern. If one needs to gain a more superior view of the interpeduncular cistern, then an orbitozygomatic craniotomy may achieve this goal without the need for a transcortical approach as proposed by the authors.

In three of the author's seven cases (two cases of a trapped temporal horn, and one of a mesial temporal AVM) the pathology was related to the temporal horn and the approach was self-evident. In the other 4 cases (three aneurysms and a craniopharyngioma) they used a combination of the transsylvian and the transinsular transchoroidal approach.

While the transsylvian trans-limen insular approach is widely known since Yasergil's publications on selective amygdalo-hippocampectomy, its use in other lesions of the perimesencephalic cisterns is not frequently encountered. The manuscript therefore is of interest as it highlights the microsurgical knowledge and decision making that such cases require.

Harry Rappaport
Ramat-Hasharon

The proposed approach could be very useful in selected cases. In my opinion it is extremely important to complete the presented studies by adding the adequate neuropsychological tests. I hope, the authors will fulfil their promise and continue the research.

Zbigniew Czernicki
Warsaw

Correspondence: Shinji Nagata, Department of Neurosurgery, Kyushu University Graduate School of Medical Sciences, 3-1-1 Maidashi Higashiku, Fukuoka 812-8582, Japan. e-mail: snagata@ns.med.kyushu-u.ac.jp

Pediatric Neurosurgery

Pediatr Neurosurg 2005;41:54–57
DOI: 10.1159/000084868

Subgaleal Dermoid Tumors at the Anterior Fontanelle

Kimiaki Hashiguchi[a] Takato Morioka[a] Nobuhiko Yokoyama[a]
Futoshi Mihara[b] Tomio Sasaki[a]

Departments of [a]Neurosurgery and [b]Clinical Radiology, Graduate School of Medical Sciences, Kyushu University, Fukuoka, Japan

Dermoid cysts at the anterior fontanelle were regarded as relatively rare, but some authors have stated that the anterior fontanelle is the most common site for dermoid cysts of the scalp [1–3]. These cysts are excised to prevent infection, obtain histological diagnosis and rule out malignancy, or for cosmetic reasons.

Three patients with subgaleal dermoid cysts over the anterior fontanelle region are described. The patients consisted of 1 male and 2 females with an age at surgery of 9, 15, and 13 months, respectively. A nontender rubbery mass in the region of the anterior fontanelle was observed in all 3 children at birth or in the first few months of life. In all cases, the tumor was slowly growing in size.

Coronal and sagittal computed tomographic (CT) scans demonstrated an extracranial low-density mass, which was assumed to be a fluid-containing cyst, in the region of the anterior fontanelle without intracranial extension. Bone density CT scans were performed to determine the topographical relationship between the tumor and anterior fontanelle. In cases 1 and 2, the anterior fontanelle was widely opened, and the tumor was located just over it as if preventing closure (fig. 1A, B, 2A). In case 3, on the other hand, at an age of 10 months the tumor was located on the frontal bone a little anterior to the anterior fontanelle (fig. 3A), and 3 months later the fontanelle was completely closed (fig. 3B, C).

Magnetic resonance images (MRIs) showed a hypointense lesion with an isointense rim on the T_1-weighted images, and a hyperintense lesion with a hypointense rim on the T_2-weighted images (fig. 1C, 2B, C, 3D), indicating the liquid character of the lesion. The tumor was not enhanced with Gd-DTPA (fig. 1D, 2D). No connection with the intracranial contents was seen.

During surgery, care should be taken while excising the tumor base if an open anterior fontanelle or erosive skull defect is observed. The simplest surgical procedure is necessary for tumor removal, and the dura should not be opened to determine a possible connection to the intracranial space, since neither intradural extension nor connection to the underlying brain have been reported [1–5]. In cases 1 and 2, the tumors were located just over the opened anterior fontanelle. They were widely attached to the dura mater, which includes the superior sagittal sinus, and therefore carefully dissected. In case 3, the tumor, which was located on the frontal skull bone just anterior to the closed anterior fontanelle, was dissected easily from the underlying skull. Total removal of the tumor was performed in all patients.

Regarding the timing of surgery, Wong et al. [5] recommend that operations should be performed after closure of the anterior fontanelle in late infancy and early childhood. However, several older infants with skull defects under a

KARGER
Fax + 41 61 306 12 34
E-Mail karger@karger.ch
www.karger.com

1016–2291/05/0411–0054$22.00/0

Accessible online at:
www.karger.com/pne

Takato Morioka, MD, PhD
Department of Neurosurgery, Graduate School of Medical Sciences, Kyushu University
3-1-1 Maidashi, Higashi-ku
Fukuoka, 812-8582 (Japan)
Tel. +81 92 642 5524, Fax +81 92 642 5526, E-Mail takato@med.kyushu-u.ac.jp

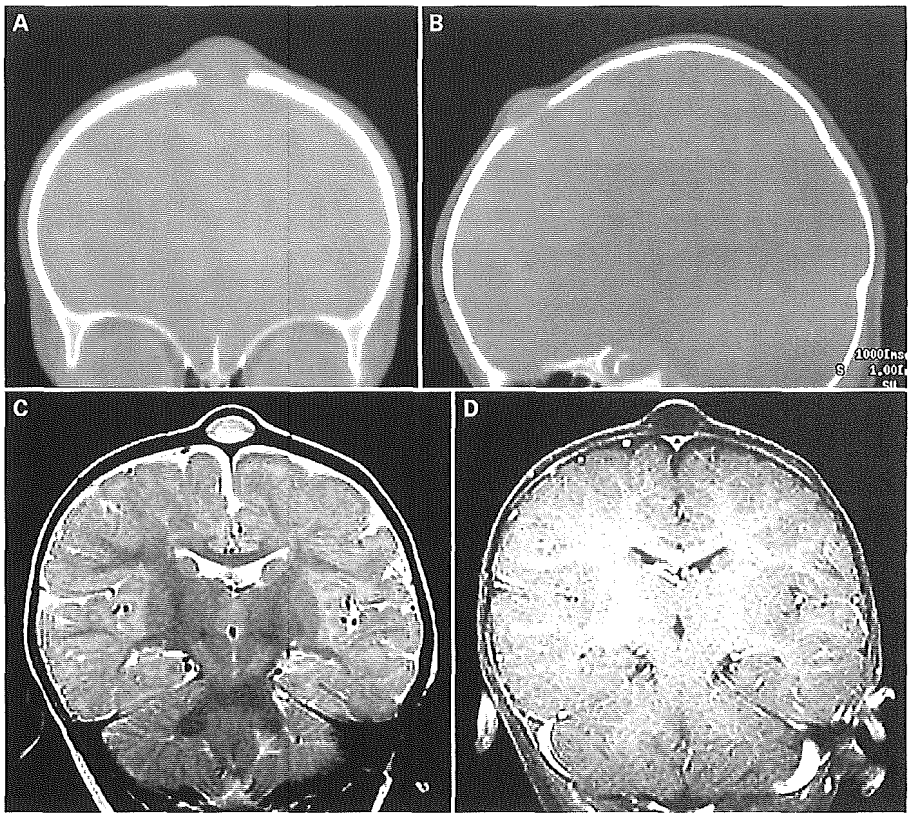

Fig. 1. Case 1 at age 9 months. Coronal (**A**) and sagittal (**B**) CT demonstrating a mass lesion located on the opened anterior fontanelle. T_2-weighted MRI demonstrating a hyperintense lesion, unconnected to the brain parenchyma or subarachnoid space (**C**). No enhancement was seen following Gd-DTPA administration (**D**).

tumor have been reported [5, 6]. Isozumi et al. [7] also reported a 35-month-old boy with a dermoid cyst over an open anterior fontanelle and widely attached to the dura mater. In our study, the 2 cases of dermoid cysts just over an open anterior fontanelle showed no changes during the several months before surgery. However, the follow-up periods of these cases were not long enough to allow evaluation of the process of change in the anterior fontanelle, although it is possible that the pressure of the cyst might have prevented the anterior fontanelle from closing.

Cysts can be located on all aspects of the anterior fontanelle [2, 3], with the anterior angle being the most common site [1, 3]. Dermoid cysts have also been reported in the midline anterior to the anterior fontanelle [2, 3]. In this study, the tumor of case 3, which involved a closed anterior fontanelle, just as those cases described above, was located on the frontal bone anterior to the anterior fontanelle. Glasauer [8] stated that dermoid cysts are commonly found a few centimeters away from the anterior fontanelle and stressed the importance of determining the different cyst locations. Dermoid cysts arising in the bones of the calvaria develop from inclusion material that proliferates within the bone, causing a gradual absorption of the adjacent bone, and producing a well-defined area of bone destruction [4]. In some previously reported cases involving a depressed outer table under the dermoid cyst, the tumors might not have originated from the anterior fontanelle, but rather from the diploe near the anterior fontanelle.

Chaudhari et al. [2] reported some causes of pronounced depression in the bone under the cysts, and the size of these cavities did not change after several months of follow-up. In their report, no direct relationship between the depth of the bone defect and the duration of the cyst was detected. With bone defects at the bregma, it is doubtful that the anterior fontanelle closes naturally, and erosive skull defects reappear later due to the pressure of the tumor. It is possible that an elongated open anterior fontanelle might develop into a bone defect.

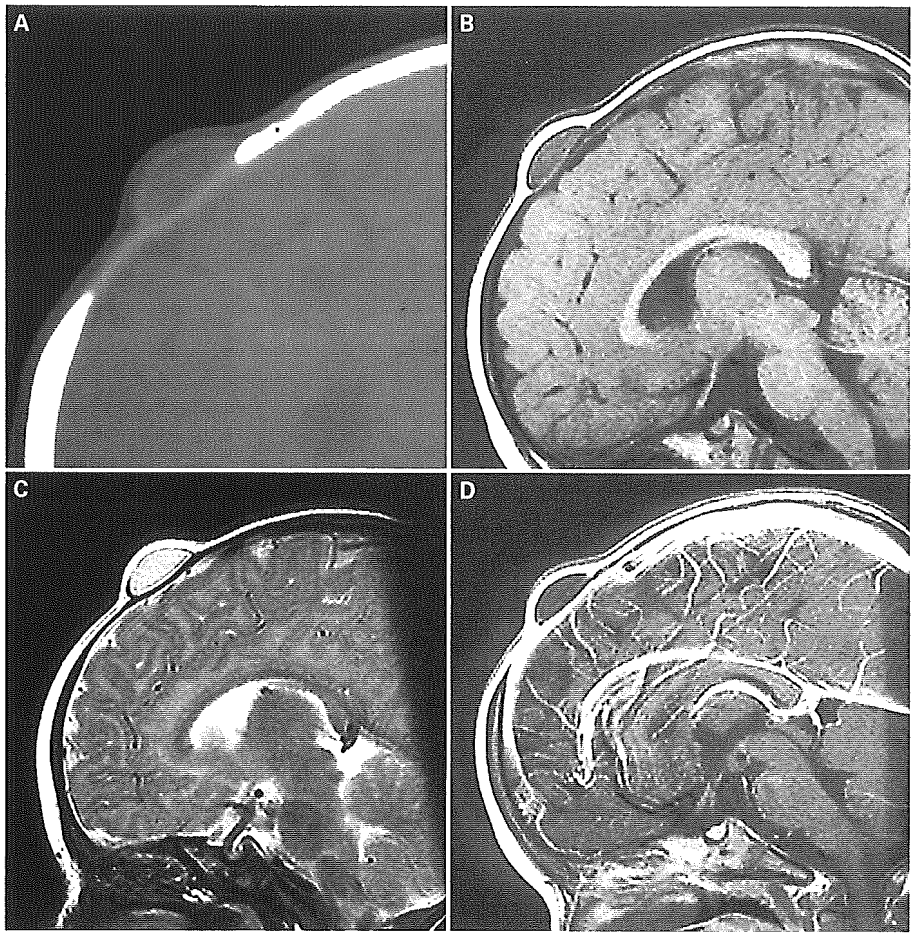

Fig. 2. Case 2 at age 15 months. Coronal CT images demonstrating a mass lesion located on the posterior part of the anterior fontanelle (**A**). The lesion is a hypointense mass on a MR T_1-weighted image (**B**) and hyperintense on a T_2-weighted image (**C**); it is unconnected to the intracranial areas. No enhancement was seen with Gd-DTPA (**D**).

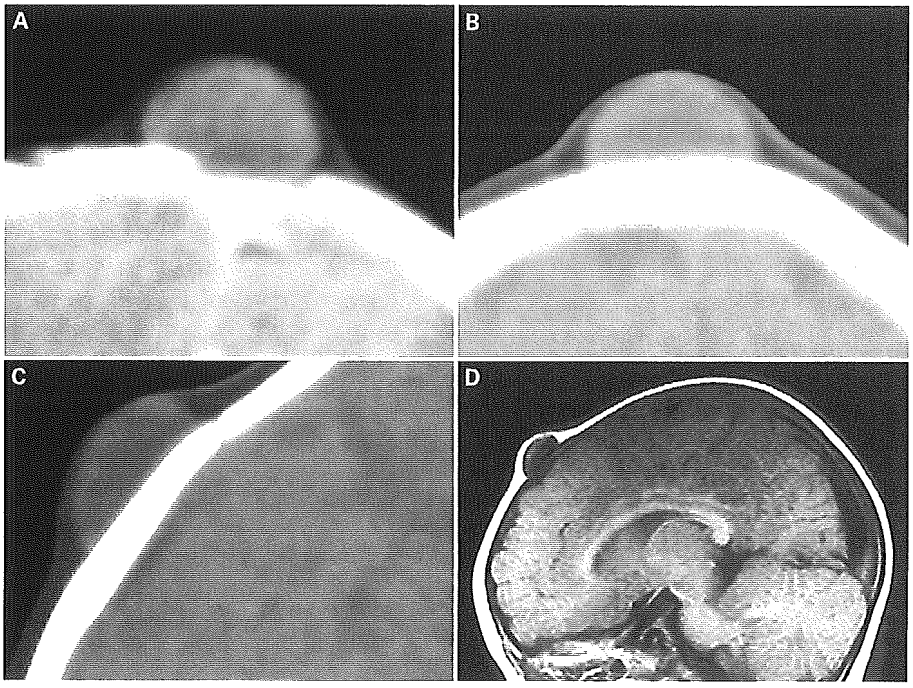

Fig. 3. Case 3 at age 9 months. Coronal CT image showing a mass lesion located on the anterior fontanelle (**A**). CT 3 months later showing that the anterior fontanelle closed and the tumor relocated to the frontal bone (**B**, **C**). T_1-weighted image demonstrating a hypointense lesion unconnected to the subarachnoid space or brain parenchyma (**D**).

References

1 Stannard MW, Currarino G: Subgaleal dermoid cyst of the anterior fontanelle: Diagnosis with sonography. AJNR Am J Neuroradiol 1990;11:349–352.

2 Chaudhari AB, Ladapo F, Mordi VPN, Choudhury KJ, Naseem A, Obe JA: Congenital inclusion cysts of the subgaleal space. J Neurosurg 1982;56:540–544.

3 Pannell BW, Hendrick EB, Hoffman HJ, Humphreys RP: Dermoid cysts of the anterior fontanelle. Neurosurgery 1982;10:317–323.

4 Glasauer FE, Levy LF, Auchterlonie WC: Congenital inclusion dermoid cyst of the anterior fontanelle. J Neurosurg 1978;48:274–278.

5 Wong T-T, Wann S-L, Lee L-S: Congenital dermoid cysts of the anterior fontanelle in Chinese children. Childs Nerv Syst 1986;2:175–178.

6 Martinez-Lage JF, Quinonez MA, Poza M, Puche A, Casas C, Costa TR: Congenital epidermoid cysts over the anterior fontanelle. Childs Nerv Syst 1985;1:319–323.

7 Isozumi T, Tsuji A, Nakasu S, Matsuda M, Handa J: Congenital dermoid cyst over the anterior fontanelle: Case report (in Japanese). No Shinkei Geka 1995;23:423–427.

8 Glasauer FE: Comments. Neurosurgery 1982; 10:323.

Clinical Chemistry 52:3
370–378 (2006)

Molecular Diagnostics and Genetics

Allelic Losses of Chromosome 10 in Glioma Tissues Detected by Quantitative Single-Strand Conformation Polymorphism Analysis

NOBUHIRO HATA,[1,2] KOJI YOSHIMOTO,[1] NOBUHIKO YOKOYAMA,[1] MASAHIRO MIZOGUCHI,[1] TADAHISA SHONO,[1] YANLEI GUAN,[1,2] TOMOKO TAHIRA,[2] YOJI KUKITA,[2] KOICHIRO HIGASA,[2] SHINJI NAGATA,[1] TORU IWAKI,[3] TOMIO SASAKI,[1] and KENSHI HAYASHI[2*]

Background: **Detection of loss of heterozygosity (LOH) in clinical tissue samples is frequently difficult because samples are usually contaminated with noncancerous cells or because tumor cells in single tissues have genetic heterogeneity, and the precision of available techniques is insufficient for reliable analysis in such materials. We hypothesized that single-strand conformation polymorphism (SSCP) analysis can precisely quantify the gene dosage in mixed samples and is suitable for detection of LOH in clinical tissue samples.**

Methods: **We assessed the accuracy of a fluorescent SSCP method for the quantification of single-nucleotide polymorphism (SNP) alleles, using DNAs that were composed of cancerous DNA mixed with noncancerous DNA at various ratios. We applied this method to precisely characterize LOH in glioma tissue samples, using 96 SNPs that were evenly distributed throughout chromosome 10.**

Results: **LOH could be detected even in the cancerous DNA heavily contaminated (up to 80%) with noncancerous DNA. Using this method, we obtained LOH profiles of 56 gliomas with resolution at the SNP level (i.e., 1.5-Mbp interval). Anaplastic astrocytomas exhibited both 10p and 10q LOH, whereas diffuse astrocytomas frequently (63% of the cases) exhibited loss of 10p alone. We also found a possible new LOH region (around 10p13) in gliomas.**

Conclusions: **The present method is effective for precise mapping of LOH region in surgically obtained tumor tissues and could be applicable to the genetic diagnosis of cancers other than gliomas.**

Loss of heterozygosity (LOH)[4] is a common genetic alteration in various kinds of cancer, and its detection is informative for diagnosis and prognosis *(1)*. In brain tumors, combined 1p and 19q LOH is a statistically significant predictor of both chemosensitivity and longer survival in patients with oligodendroglial tumors *(2, 3)*. In general, LOH is a genetic alteration that leads to the inactivation of tumor suppressor genes and is considered to be a critical event in cancer development *(4)*. Thus, mapping of LOH regions is a practical approach to the identification of genes whose loss is related to tumorigenesis *(5)*.

LOH on chromosome 10 is the most frequent genetic alteration in glioblastomas (GBMs), which are the most malignant grade of gliomas according to WHO criteria *(6, 7)*. Investigation of segmental LOH on chromosome 10 in GBMs has revealed at least 3 common LOH regions: 10p14–15, 10q23–24, and 10q25–26 *(8–14)*. It has therefore been suggested that multiple tumor suppressor genes exist on chromosome 10. The *PTEN* gene at 10q23 has been identified as a tumor suppressor gene in GBM *(15, 16)*. The significance of LOH in the other chromosome 10 regions, however, is still controversial. Thus,

Departments of [1] Neurosurgery and [3] Neuropathology, Graduate School of Medical Sciences, and [2] Division of Genome Analysis, Research Center for Genetic Information, Medical Institute of Bioregulation, Kyushu University, Fukuoka, Japan.

* Address correspondence to this author at: Division of Genome Analysis, Research Center for Genetic Information, Medical Institute of Bioregulation, Kyushu University, Maidashi 3-1-1, Higashi-ku, Fukuoka 812-8582, Japan. Fax 81-92-632-2375; e-mail khayashi@gen.kyushu-u.ac.jp.

Received September 25, 2005; accepted December 8, 2005.
Previously published online at DOI: 10.1373/clinchem.2005.060954

[4] Nonstandard abbreviations: LOH, loss of heterozygosity; GBM, glioblastoma; SNP, single-nucleotide polymorphism; SSCP, single-strand conformation polymorphism; LOQUS, LOH estimation by quantitative SSCP analysis; AA, anaplastic astrocytoma; DA, diffuse astrocytoma; and SSC, standard saline citrate.

detailed mapping of LOH regions is important to clarify the mechanism of malignant glioma formation.

Although conventional LOH studies have used allelotyping with microsatellite markers, these methods are not sufficient for the identification of specific genes because of the low density of the available markers. On the other hand, single-nucleotide polymorphisms (SNPs) are the most abundant form of sequence variations in the human genome *(17)*, and worldwide efforts to collect SNPs have led to the accumulation of millions of these polymorphisms in public databases. Because of their overwhelming abundance in the genome, SNPs can serve as the basis for a high-density LOH analysis method. Many SNP-genotyping methods have been developed, and some of them can be applied to detect LOH *(18, 19)*. A quantitative SNP genotyping method using an oligonucleotide array, called WGSA, detects LOH with high resolution. The detection rate of LOH, however, is lower for DNA samples extracted from heterogeneous tumor tissue because of contamination by nonmalignant cells *(20)*.

In gliomas, diffuse infiltration is frequently observed independent of histologic grade, and the tumor tissue is not demarcated from noncancerous tissue *(21)*. Tolerance to contamination by noncancerous cells is therefore essential for LOH analysis of glioma samples. We previously developed a SNP-genotyping method, PLACE-SSCP, in which PCR products are postlabeled with fluorescent dyes and labeled products are analyzed in an automated capillary electrophoresis system under single-strand conformational polymorphism (SSCP) analysis conditions *(22, 23)*. In this system, precise quantification of allele frequencies of SNPs is possible with use of pooled DNA samples *(24)*.

In the present study, we explored the effectiveness of PLACE-SSCP for detecting allelic imbalance and developed a new sensitive approach, LOH estimation by quantitative SSCP analysis (LOQUS), to detect LOH at the SNP resolution level. We first evaluated the high sensitivity of this analysis, using a tumor cell line DNA artificially mixed with DNA from noncancerous cells. Subsequently, we analyzed LOH on chromosome 10 in glioma samples and investigated the correlation between the LOH profile and histologic grade. This method revealed a new LOH hot spot at 10p13, which is a putative area that may harbor tumor suppressor genes.

Materials and Methods

SAMPLES AND DNA PREPARATION

Glioma samples were obtained from patients during surgery at Kyushu University Hospital or other affiliated institutions. A part of the tumor tissue was saved for histopathologic examination; the rest was snap-frozen in liquid nitrogen and stored at −80 °C. Tumors were histologically diagnosed by a qualified neuropathologist and graded according to the WHO criteria *(21)*. Tumor tissue samples were collected from 56 patients with gliomas, including 35 GBMs, 8 anaplastic astrocytomas (AAs), 8 diffuse astrocytomas (DAs), and 5 gliomas categorized as WHO grade I (3 pilocytic astrocytomas, 1 pilomyxoid astrocytoma, and 1 ganglioglioma). Among them, 13 GBMs were used in a previous study of LOH analysis with microsatellite markers *(25)*. Tumor DNA was isolated from the frozen blocks by a standard phenol–chloroform extraction procedure. Corresponding wild-type DNA was isolated from a blood sample from the same patient by use of a QIAamp DNA Blood Kit (Qiagen). The present investigation was approved by the Ethics Committee of Kyushu University.

SINGLE-NUCLEOTIDE POLYMORPHISMS

We chose 384 SNPs on chromosome 10 from public databases: JSNP (http://snp.ims.u-tokyo.ac.jp/), TSC (http://snp.cshl.org/), and NCBI dbSNP (http://www.ncbi.nlm.nih.gov/SNP/). The frequencies of the minor alleles for the chosen SNPs were >20% in Japanese or Asians in at least one of the above public databases. Among them, 288 SNPs were mapped to the distal portion of chromosome 10q (10q25-telomeric end), and 96 SNPs were from other regions of chromosome 10. The genomic sequences including the chosen SNPs were downloaded from NCBI (http://www.ncbi.nlm.nih.gov/), and the repetitive sequences were masked by use of *Repeatmasker* (http://www.repeatmasker.org/). PCR primer pairs for all SNPs were designed for the nonredundant regions by use of *Primer3* software *(26)* to obtain a product of 80 to 300 bp and a standardized primer melting temperature (T_m) of 55–65 °C. Oligonucleotide primer pairs (custom synthesized at SIGMA Genosys, Hokkaido, Japan) were made to carry either 5′-ATT or 5′-GTT for postlabeling purposes, as described previously *(22)*.

PCR

PCR was performed in a total volume of 5 μL containing 25 ng of template DNA, 0.25 μM each of the primers, 0.2 mM each of the nucleotides, 0.125 U of AmpliTaq® DNA polymerase (Applied Biosystems), 27.5 ng of TaqStart™ antibody (Clontech Laboratories), 2 mM $MgCl_2$, 10 mM Tris-HCl (pH 8.3), 50 mM KCl, and 50 nL/μL dimethyl sulfoxide. The thermal cycle profile was 1 min at 94 °C for initial heating, followed by 40 cycles of 30 s at 94 °C, 30 s at 60 °C, and 1 min at 72 °C.

PLACE-SSCP AND DATA ANALYSIS

Post-PCR labeling was performed, followed by removal of the residual fluorescent nucleotides by gel filtration, as described previously *(23)*. Electrophoresis was performed under SSCP conditions in a 36-cm capillary in the ABI Prism® 3100 genetic analyzer (Applied Biosystems). The samples were dissolved in 0.5 mmol/L EDTA, loaded by electrokinetic injection at 2 kV for 10 s, and separated at 15 kV for 30 min, as described previously *(27)*. Output data

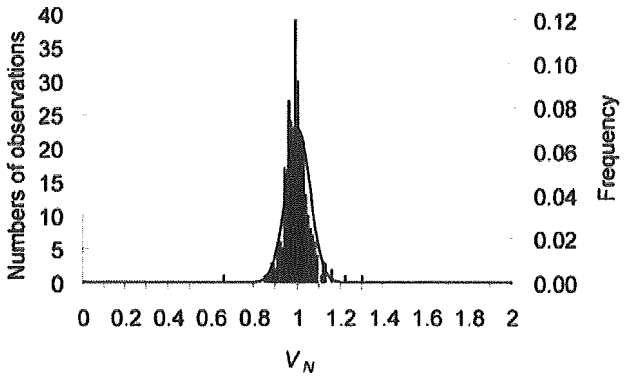

Fig. 1. Distributions of run-to-run variability of the peak-height ratio (V_N) of the 2 alleles in heterozygous samples.

The peak-height ratio (R_N) of every sample heterozygous for all SNPs was determined in duplicate runs. The ratio of R_N for the duplicates (V_N) was then calculated. *Columns* indicate the numbers of observed V_N within the bins of width (V_N) 0.05. The *curve* shows the approximated gaussian distribution, in which the mean (SD) was 1.000 (0.057).

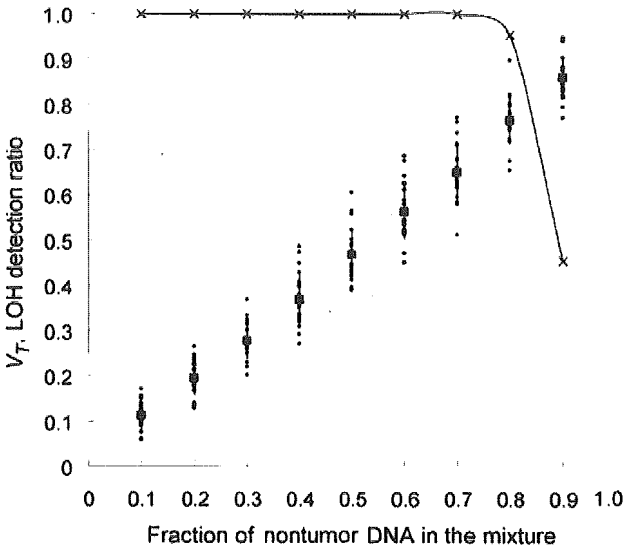

Fig. 2. LOH analysis using mixed samples.

The *x axis* shows the fraction of nontumor DNA in the mixture. The *y axis* shows V_T value or LOH detection rate. Each ● represents V_T for each locus (22 loci) across the 9 different mixing ratios. ■ and *vertical lines* indicate mean (SD) values of V_T. × indicate LOH detection rates, which were determined as the fraction of SNPs for which V_T was <0.83. See text for the definition of V_T.

were converted to ASCII format and then imported to Quantitative Interpretation of SSCP in Capillary Array (QUISCA) software for analysis *(23, 28)*.

DNA FOR MIXING EXPERIMENT

We purchased DNA samples extracted from a non-small lung cancer cell line (NCI-H2126) and its matched non-cancer cell line (NCI-BL2126) from the American Type Culture Collection. The DNA concentrations were determined by use of a PicoGreen ds-DNA quantification assay (Molecular Probes), and paired DNA of equal concentration was obtained by diluting with 0.1× Tris-EDTA buffer. The tumor DNA was then diluted with NCI-BL2126 DNA of the same concentration in 10% increments.

FLUORESCENT IN SITU HYBRIDIZATION

Imprint preparations of tumor cells were prepared from unfixed snap-frozen samples, as described previously with some modifications *(29)*. In brief, small pieces of cancer tissue were touched against silanized slides, and the slides were fixed 3 times in methanol–acetic acid (3:1 by volume) for 10 min each and subsequently air-dried. Cells on slides were denatured in 700 mL/L formamide in 2× standard saline citrate (SSC; pH 7) at 75 °C for 5 min. After dehydration in an ethanol series (700 mL/L, 850 mL/L, and absolute ethanol), samples were treated with 0.1 g/L proteinase K (Merck) in phosphate-buffered saline (pH 7) at 37 °C for 3 min, followed by a second dehydration in ethanol. Hybridization was performed with the LSI PTEN/CEP 10 Dual Color Probe, which is a mixture of a locus-specific probe (LSI) localized on band 10q23 and a subcentromeric probe (CEP) on band 10p11.1-q11.1 (Vysis). The probe mixture was denatured at 73 °C for 5 min and hybridized to the denatured cells on the slides. After cells were covered with an 18 × 18 mm coverslip and sealed with rubber cement, hybridization was allowed to proceed for 2 days. Slides were then washed twice at room temperature for 5 min in 2× SSC containing 3 mL/L NP-40, then at 73 °C for 2 min. After washing, nuclei were counterstained with 0.15 mg/L 4.5-diamino-2-phenyl-indole. Slides were scored for the number of fluorescent signals in each nucleus by use of a Zeiss Axioskop 2 plus fluorescence microscope equipped with a triple-pass filter (Aqua/Green/Orange; Vysis).

MICROSATELLITE ANALYSIS

Tumor and nontumor DNAs were evaluated by a PCR-based LOH assay using 8 microsatellite markers located at regions on chromosome 10 frequently deleted in gliomas (D10S591, D10S1649, D10S1652, D10S1765, D10S587, D10S216, D10S217, and D10S1655). PCR and fluorescence labeling were performed according to a previously described method *(25)*. Capillary electrophoresis was performed with a 310 Prism Genetic Analyzer (Applied Biosystems). Raw electrophoresis data were analyzed with GeneScan Analysis software (Applied Biosystems). Allelic status was assessed based on the criteria established in a previous study *(25)*. Microsatellite instability was determined by the appearance of extra bands on tumor DNA examination.

Results

SELECTION OF SNP MARKERS

We tested the effectiveness of PLACE-SSCP by assessing the LOH status of chromosome 10, which is the site of one of the most frequent genetic alterations associated with malignant gliomas *(6, 7)*. We first chose 384 SNP markers

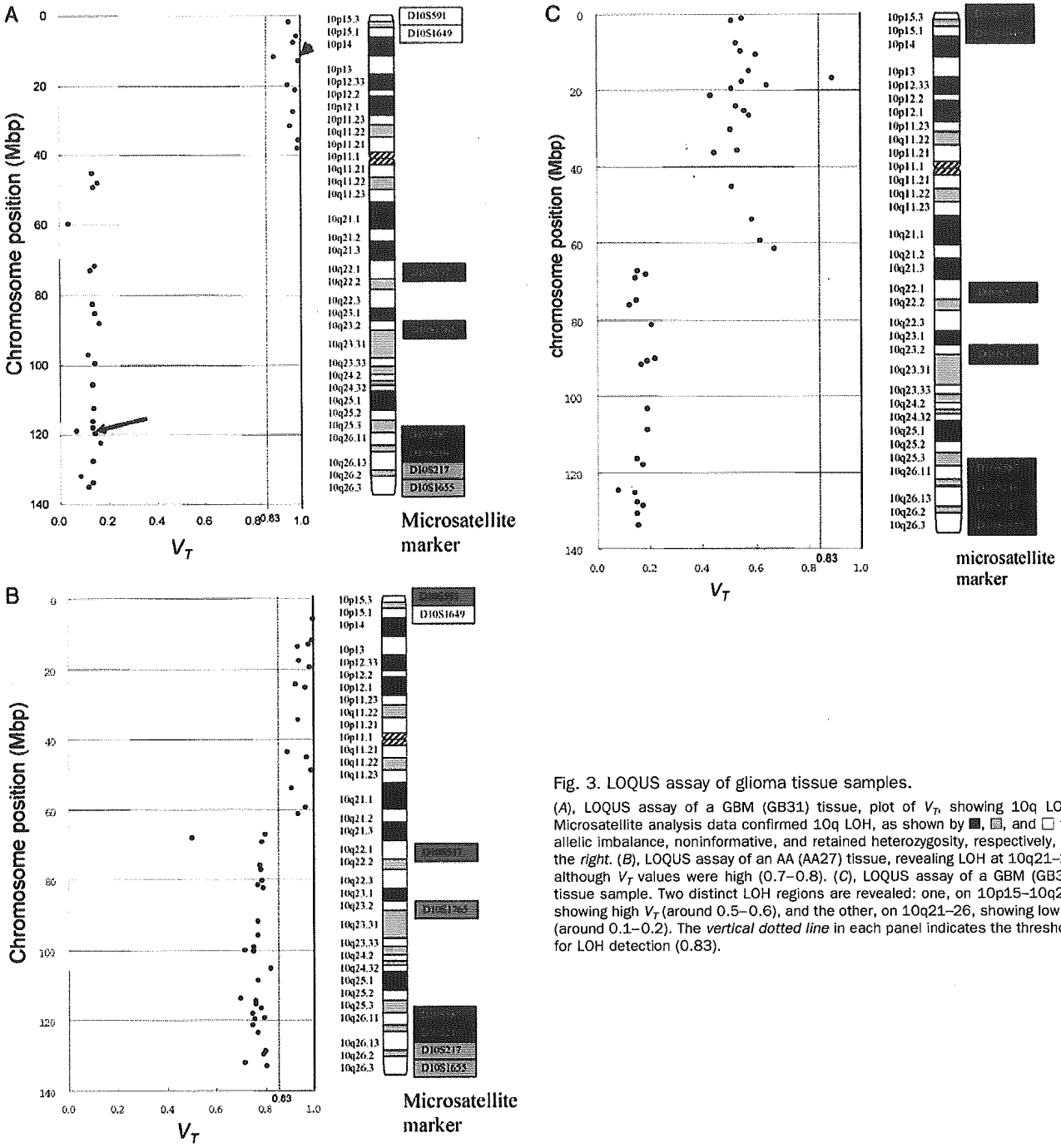

Fig. 3. LOQUS assay of glioma tissue samples.

(*A*), LOQUS assay of a GBM (GB31) tissue, plot of V_T, showing 10q LOH. Microsatellite analysis data confirmed 10q LOH, as shown by ■, ▨, and □ for allelic imbalance, noninformative, and retained heterozygosity, respectively, on the *right*. (*B*), LOQUS assay of an AA (AA27) tissue, revealing LOH at 10q21–26 although V_T values were high (0.7–0.8). (*C*), LOQUS assay of a GBM (GB35) tissue sample. Two distinct LOH regions are revealed: one, on 10p15–10q21, showing high V_T (around 0.5–0.6), and the other, on 10q21–26, showing low V_T (around 0.1–0.2). The *vertical dotted line* in each panel indicates the threshold for LOH detection (0.83).

on chromosome 10 as described in the *Materials and Methods*, and PCR reactions on tumor and corresponding nontumor DNA were performed for each sequence-tagged site containing a SNP in the same batch. Subsequently, PCR products were divided and used for sequencing and PLACE-SSCP analyses for the same 8 individuals, and these data were interpreted independently. Among the 384 SNPs, a total of 70 (18.2%) were excluded from further analysis because the peak patterns of the SSCP analyses were not interpretable (22 SNPs), separation of allele peaks of heterozygous samples was insufficient for quantitative SSCP analysis (28 SNPs), or there was no heterozygote sequenced among the 8 individuals (20 SNPs). From the remaining 314 SNPs, we excluded SNPs with a minor allele frequency <30% in the 8 individuals. The 96 SNPs that distributed evenly throughout chromosome 10 (marker intervals ~1.5 Mbp) were used for subsequent analyses.

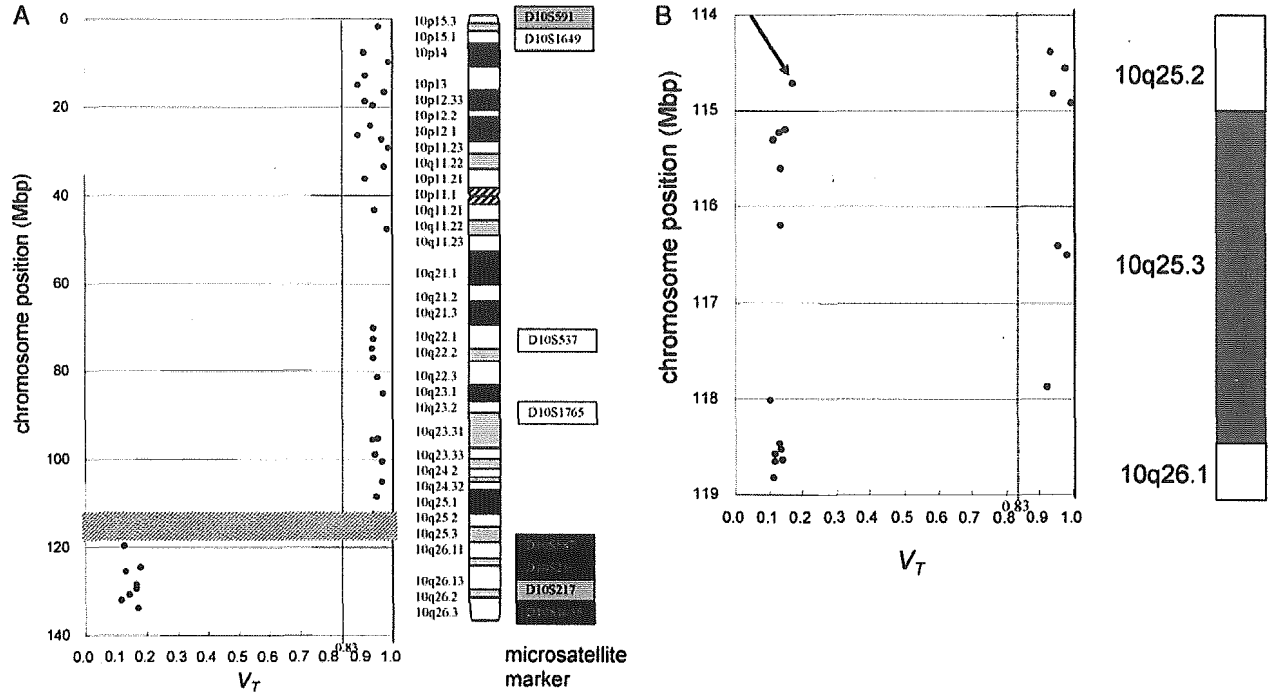

Fig. 4. LOQUS assay of an AA sample (AA24).

(*A*), LOH at a region distal to 10q, obtained with the set of 96 SNPs. is shown (*B*), *hatched region* in *A* (from 114 to 119 Mbp of chromosome 10) was analyzed further by use of high-density SNPs. There is a single LOH locus, rs720785 (*arrow*), at chromosome position 114 711 558 bp, disrupting the 2 regions of retained heterozygosity, indicating the presence of an LOH region <250 kbp in length. Another LOH region of ~1.5 Mbp on the chromosome region around 116 Mbp was also detected. The *vertical dotted line* in each *panel* indicates the threshold for LOH detection (0.83).

REPRODUCIBILITY OF PEAK-HEIGHT RATIOS OF ALLELES IN NONTUMOR CELLS FROM PERSONS HETEROZYGOUS FOR SNPs

The sensitivity of LOH detection by PLACE-SSCP depends on the accuracy of the estimation of relative allele abundance in the samples, which in turn depends on the reproducibility of peak-height ratios of alleles in either nontumor cells from individuals heterozygous for the SNP being evaluated or in tumor samples. We defined R_N as the height ratio of the peak for the first allele peak to the peak for the second allele in nontumor DNA from individuals heterozygous for each SNP. For each SNP, PCR reactions from the same DNA were performed in 2 wells of the same microtiter plate, and 2 R_N values (R_{N1} and R_{N2}) were obtained for all SNPs in nontumor cells showing heterozygosity. We analyzed the 96 SNPs, using nontumor DNA from 8 heterozygous individuals, and determined the variability of the peak-height ratio obtained for the same nontumor DNA (V_N) by R_{N1}/R_{N2} for all SNPs showing heterozygosity (326 determinations). The mean (SD) V_N was 1.000 (0.057), with a CV of 5.7%, and the data were fitted to a gaussian distribution by use the Shapiro–Wilk *W* test with JMP software (Ver. 5.0.1J; SAS Institute; http://www.sas.com/; Fig. 1) (*30*). The test revealed a gaussian distribution (W = 0.9626) with high significance (P <0.0001). We define V_T [min(R_T/R_N, R_N/R_T)] as an indicator of the fraction of the DNA with allelic imbalance in the tumor sample, where R_T is the peak height ratio of the tumor sample (see Fig. 2 of the Data Supplement that accompanies the online version of this article at http://www.clinchem.org/content/vol52/issue3/). We thus conclude that V_T <0.83 (3 SD from the mean) can be regarded as an LOH at a confidence level of ~99.7% (according to the probability density of the gaussian distribution). We adopted this criterion as an indication of LOH in the LOQUS assay described below.

MIXED DNA EXPERIMENT

Glioma tissue samples frequently show heterogeneity or infiltration by noncancerous cells. To further estimate the sensitivity of LOQUS to detect the allelic status in such situations, we performed reconstitution experiments in which a pair of DNA samples from tumor and healthy tissues of the same individual were mixed at various ratios and subjected to LOQUS analyses. The DNA samples for this experiment were obtained from a lung cancer cell line (NCI-H2126) and its matched noncancer cell line DNA (NCI-BL2126), in which LOH was detected in all informative microsatellite markers examined on chromosome 10 (*31*). Among the 96 SNPs, SSCP analysis of NCI-BL2126 indicated heterozygosity for 22. The LOQUS assay performed with these SNPs indicated that V_T increased proportionally in response to an increase in nontumor DNA (Fig. 2). At a mixing ratio of 20 (i.e., 20% tumor DNA and 80% nontumor DNA), LOH was detectable in 95% of the examined SNPs (21 of 22), and above

this ratio (>20% tumor DNA), LOH was detected with every SNP. Even at a 10% mixing ratio, LOH was still detectable for 10 of 22 SNPs (46%). These results indicate that the LOQUS assay can tolerate a mixed sample contaminated with up to 80% noncancer DNA.

LOQUS ASSAY IN GLIOMA TISSUE SAMPLES

We performed the LOQUS assay with glioma tissue samples. The result of examination of a GBM sample (GB31), in which LOH of the entire 10q was detected, is shown in Fig. 3A. This LOH was confirmed by both microsatellite markers and fluorescence in situ hybridization analyses (see Fig. 1 in the online Data Supplement). We could also detect LOH on 10q in samples for which the V_T values were in the range 0.7–0.8 (Fig. 3B). The results obtained for an AA sample (AA24), in which a microdeletion measuring <250 kbp was detected by narrowing the region of analysis by use of densely located SNPs, are shown in Fig. 4.

LOH PROFILES OF CHROMOSOME 10 IN GLIOMAS

We analyzed 56 glioma samples, and the mean number of informative loci was 40.91 (42% of examined SNPs). LOH profiles of examined samples are shown in Fig. 3 of the online Data Supplement. The majority of GBMs (68%) had LOH at all informative loci, and were therefore interpreted to be a monosomy of chromosome 10. In contrast, AAs and low-grade gliomas showed no such LOH pattern, except for 1 AA sample. LOH on 10q was observed in all of the AA cases, and their LOH regions included multiple loci. On the other hand, all LOH on 10q observed in DAs and grade I gliomas involved loss of a single region. LOH on 10p was observed in 63% of DAs and AAs, whereas none of the grade I gliomas had LOH in this chromosome region. As for DAs, LOH on 10p included multiple loci, in contrast to LOH on 10q.

IDENTIFICATION OF AN LOH HOT SPOT AT 10p13

Among the 56 gliomas, the LOH ratio (ratio of samples with LOH to all informative samples) of 96 SNPs varied from 40% (rs724444 at chromosome position 77 558 207 bp) to 77.8% (rs726451 at chromosome position 122 403 971 bp). On the basis of the LOH ratio plot shown in Fig. 5, we identified 3 LOH hot spots: 10p13–15, the *PTEN* region at 10q23, and 10q25–26. The latter 2 regions were consistent with the previously reported commonly deleted lesions in malignant gliomas *(8, 11, 12)*. The first deletion hot spot overlapped the commonly deleted region (10p14–15) reported in other studies *(9, 10, 14)*, but somewhat extended to the centromeric side. We therefore focused on the 10p LOH samples. To identify the minimal 10p LOH region, we compared 40 samples with at least one LOH locus on 10p: 30 GBMs, 5 AAs, and 5 DAs (Fig. 6). We found that 2 samples (GB9 and DA23) had an interstitial LOH localized at the centromeric portion of 10p13, and all informative samples showed LOH of rs1376690 at chromosome position 15 720 079 bp.

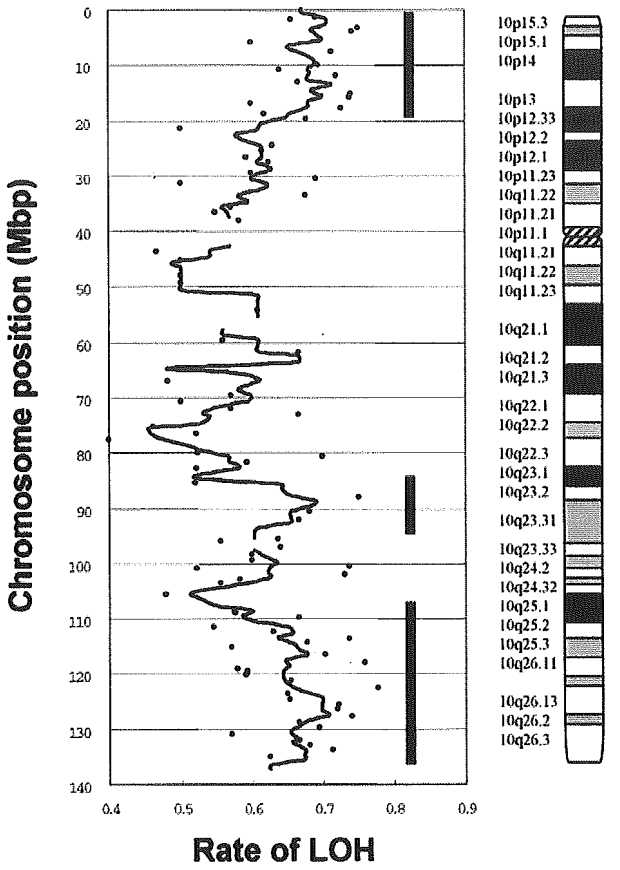

Fig. 5. LOH data for the analyzed samples.

LOH fractions in 56 glioma samples are shown. ● indicate the rate of LOH for each locus, and the *horizontal lines* indicate the moving average in 5 Mbp windows. The *vertical bars* show the 3 common LOH regions: 10p13–15, 10q23, and 10q25–26.

We are currently performing investigations to identify genes possibly involved in the development of gliomas.

Discussion

Traditionally, LOH has been estimated by detecting allelic imbalance by use of microsatellite markers. The use of SNP markers for LOH detection has the advantage of much higher resolution because SNPs are available at an overwhelmingly higher density. The results are also more reliable because SNPs are more stable markers than microsatellites in vivo and microsatellite instability during tumor evolution or formation is avoided. Slippage during PCR and the appearance of stutter peaks are frequently encountered problems of microsatellite analysis, which does not exist for SNP markers.

We demonstrated high reproducibility (CV = 5.7%) of the signal intensity ratio of SNP alleles in the analysis of DNA from samples heterozygous for the SNPs studied in the LOQUS analysis. This reproducibility is comparable to that of the bacterial artificial chromosome–based comparative genomic hybridization array *(32, 33)* and better

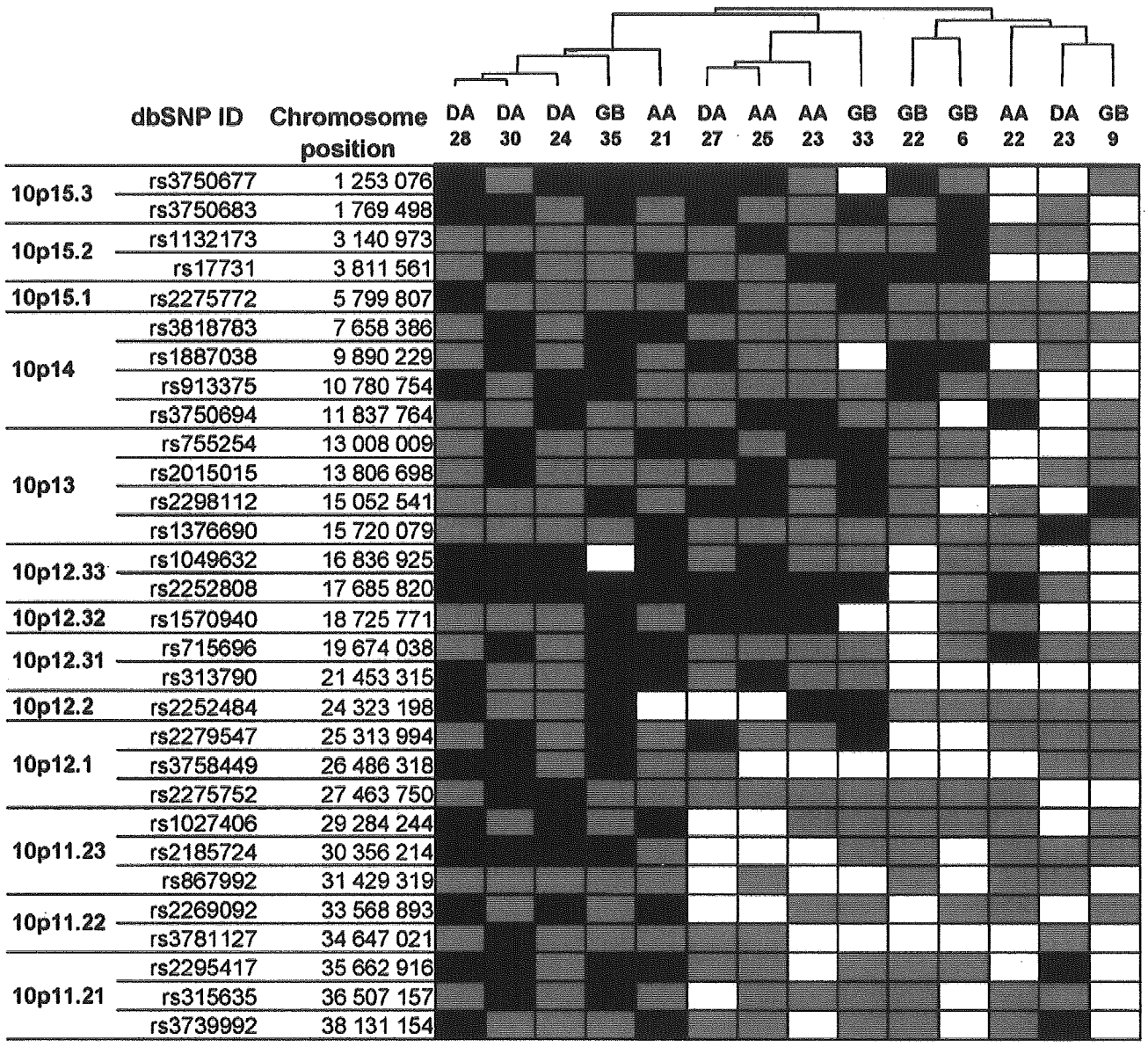

Fig. 6. Summary of 10p LOH regions in glioma samples.

The Ward method *(40)* was used for hierarchical clustering of samples by use of JMP software. The samples with LOH at all informative loci, which were interpreted to be a monosomy of chromosome 10, or retention of heterozygosity at all informative loci, were excluded. SNP markers are shown on the *left*. Case numbers are indicated at the *top*. ■, LOH; □, retention of heterozygosity; ▨, not informative (homozygous individual or not determined).

than the reproducibility of other methods such as multiplex ligation–dependent probe amplification analysis *(34, 35)*, multiplex amplification and probe hybridization analysis *(36)*, and SYBR Green I–based real-time PCR analysis *(30)*.

Recently, oligonucleotide microarray analysis was applied to detect LOH at the SNP level *(19, 37)*. As an advantage of this method, both LOH and the copy number abnormality profile can be determined by single-platform analysis. Although oligonucleotide microarrays allow high-throughput analysis, their use requires a relatively high proportion of tumor DNA to detect LOH. When contamination by noncancer DNA reaches 30%–50% of the total, there is a significant loss of detection of LOH by the microarray analysis *(20)*. In contrast, the reproducibility of the peak-height ratio for SNP alleles obtained with the LOQUS method is high, as shown in Fig. 1, and this method can tolerate a mixed sample with up to 80% contamination by DNA from noncancerous cells and still detect an allelic imbalance. For specimen with a low percentage of tumor cells, further experiments, e.g., microdissection to enrich tumor cells, should provide more convincing results on the determination of LOH status.

Contamination by nontumor cells in tumor tissue samples is inevitable because contribution of ancillary cells such as fibroblasts and endothelial cells is essential for tumor maintenance, and they frequently infiltrate the tissue *(38)*. Although methods such as culturing or laser capture microdissection have been used to enrich tumor cell content, obtaining pure tumor cell populations remains difficult. Furthermore, based on the clonal multistep tumor evolution theory, tumor cells do not have a uniform genetic change in clinical tumor tissues *(39)*. The LOQUS assay also can detect the heterogeneity of tumor cells, as shown in Fig. 3C, which revealed 2 distinct LOH regions showing high and low V_T. These results demonstrate the robustness of our method in the examination of clinically obtained tumor tissue samples, which are often mixed with an excess of healthy cells or consist of a heterogeneous population of 2 or more malignant cell types.

Other advantages of our method, as well as other targeted methods such as multiplex ligation–dependent probe amplification or multiplex amplification and probe hybridization analysis, over microarray-based genome-wide methods are flexibility of experimental design and the cost of analysis. LOQUS analysis requires only widely available instrumentation, i.e., a conventional PCR instrument and capillary sequencer. The throughput of this system is low compared with other methods, e.g., microarray-based techniques. Use of the ABI Prism® 3100 genetic analyzer, which is the most appropriate instrument for PLACE-SSCP *(27)*, enables analysis of 96 loci in 1 day, including PCR steps. However, PLACE-SSCP has the advantage of flexibility, e.g., additional high-density investigations could be done simply by selecting additional SNPs from public databases and designing the appropriate PCR primers. The recent enhancement of public databases allows selection of SNPs with high heterozygosity, which is essential for efficient analysis of allelic imbalance using the present system.

The LOH profiles in the present study indicated the following: (*a*) The majority of the GBMs had complete LOH of chromosome 10. (*b*) AAs frequently had partial LOH on both 10p and 10q. (*c*) DAs also frequently had 10p LOH, but seldom had 10q LOH. The progression of astrocytoma is associated with an increased loss of 10p and 10q sequences, probably reflecting the increased involvement of tumor suppressor genes *(14)*. Our findings are consistent with these observations and, in addition, suggest that 10p LOH has a less malignant effect compared with 10q LOH in glioma formation or progression.

According to previous microsatellite analyses of astrocytic gliomas with different malignancy grades, 10p LOH is frequently observed in a subpopulation of tumor cells *(9)*. Such subtle genetic abnormalities are more reliably detected by a highly sensitive method such as LOQUS. Moreover, the higher frequency of 10p LOH in DAs detected in this study (63%) compared with previous reports (0%–35%) *(9, 10, 14)* might be attributable to the high sensitivity of the present method.

The reported regions on 10p commonly deleted in gliomas are concentrated at 10p14–15 *(9, 10, 14)*. We identified an additional deletion hot spot at 10p13, however, suggesting that 10p13 is an additional putative area that might harbor previously undiscovered tumor suppressor genes. Further efforts are needed to identify genes at deletion hot spots on chromosome 10, including 10p13, to elucidate the significance of LOH in chromosome 10 regions in gliomas.

References

1. Thiagalingam S, Foy RL, Cheng KH, Lee HJ, Thiagalingam A, Ponte JF. Loss of heterozygosity as a predictor to map tumor suppressor genes in cancer: molecular basis of its occurrence. Curr Opin Oncol 2002;14:65–72.
2. Cairncross JG, Ueki K, Zlatescu MC, Lisle DK, Finkelstein DM, Hammond RR, et al. Specific genetic predictors of chemotherapeutic response and survival in patients with anaplastic oligodendrogliomas. J Natl Cancer Inst 1998;90:1473–9.
3. Smith JS, Perry A, Borell TJ, Lee HK, O'Fallon J, Hosek SM, et al. Alterations of chromosome arms 1p and 19q as predictors of survival in oligodendrogliomas, astrocytomas, and mixed oligoastrocytomas. J Clin Oncol 2000;18:636–45.
4. Cavenee WK, Dryja TP, Phillips RA, Benedict WF, Godbout R, Gallie BL, et al. Expression of recessive alleles by chromosomal mechanisms in retinoblastoma. Nature 1983;305:779–84.
5. Lasko D, Cavenee W, Nordenskjold M. Loss of constitutional heterozygosity in human cancer. Annu Rev Genet 1991;25:281–314.
6. Kleihues P, Cavenee WK. World Health Organization classification of tumors: tumors of the nervous system. Lyon, France: IARC Press, 2000:29–39.
7. Maher EA, Furnari FB, Bachoo RM, Rowitch DH, Louis DN, Cavenee WK, et al. Malignant glioma: genetics and biology of a grave matter. Genes Dev 2001;15:1311–33.
8. Fujisawa H, Reis RM, Nakamura M, Colella S, Yonekawa Y, Kleihues P, et al. Loss of heterozygosity on chromosome 10 is more extensive in primary (de novo) than in secondary glioblastomas. Lab Invest 2000;80:65–72.
9. Ichimura K, Schmidt EE, Miyakawa A, Goike HM, Collins VP. Distinct patterns of deletion on 10p and 10q suggest involvement of multiple tumor suppressor genes in the development of astrocytic gliomas of different malignancy grades. Genes Chromosomes Cancer 1998;22:9–15.
10. Kimmelman AC, Ross DA, Liang BC. Loss of heterozygosity of chromosome 10p in human gliomas. Genomics 1996;34:250–4.
11. Maier D, Zhang Z, Taylor E, Hamou MF, Gratzl O, Van Meir EG, et al. Somatic deletion mapping on chromosome 10 and sequence analysis of PTEN/MMAC1 point to the 10q25–26 region as the primary target in low-grade and high-grade gliomas. Oncogene 1998;16:3331–5.
12. Mohapatra G, Bollen AW, Kim DH, Lamborn K, Moore DH, Prados MD, Feuerstein BG. Genetic analysis of glioblastoma multiforme provides evidence for subgroups within the grade. Genes Chromosomes Cancer 1998;21:195–206.
13. Steck PA, Lin H, Langford LA, Jasser SA, Koul D, Yung WK, et al. Functional and molecular analyses of 10q deletions in human gliomas. Genes Chromosomes Cancer 1999;24:135–43.
14. Voesten AM, Bijleveld EH, Westerveld A, Hulsebos TJ. Fine

mapping of a region of common deletion on chromosome arm 10p in human glioma. Genes Chromosomes Cancer 1997;20:167–72.

15. Li J, Yen C, Liaw D, Podsypanina K, Bose S, Wang SI, et al. PTEN, a putative protein tyrosine phosphatase gene mutated in human brain, breast, and prostate cancer. Science 1997;275:1943–7.
16. Steck PA, Pershouse MA, Jasser SA, Yung WK, Lin H, Ligon AH, et al. Identification of a candidate tumour suppressor gene, MMAC1, at chromosome 10q23.3 that is mutated in multiple advanced cancers. Nat Genet 1997;15:356–62.
17. Reich DE, Gabriel SB, Altshuler D. Quality and completeness of SNP databases. Nat Genet 2003;33:457–8.
18. Barrett MT, Scheffer A, Ben-Dor A, Sampas N, Lipson D, Kincaid R, et al. Comparative genomic hybridization using oligonucleotide microarrays and total genomic DNA. Proc Natl Acad Sci U S A 2004;101:17765–70.
19. Bignell GR, Huang J, Greshock J, Watt S, Butler A, West S, et al. High-resolution analysis of DNA copy number using oligonucleotide microarrays. Genome Res 2004;14:287–95.
20. Huang J, Wei W, Zhang J, Liu G, Bignell GR, Stratton MR, et al. Whole genome DNA copy number changes identified by high density oligonucleotide arrays. Hum Genomics 2004;1:287–99.
21. Kleihues P, Cavenee WK. World Health Organization classification of tumors. Tumors of the nervous system. Lyon, France: IARC Press, 2000:10–21.
22. Inazuka M, Wenz HM, Sakabe M, Tahira T, Hayashi K. A streamlined mutation detection system: multicolor post-PCR fluorescence labeling and single-strand conformational polymorphism analysis by capillary electrophoresis. Genome Res 1997;7:1094–103.
23. Kukita Y, Higasa K, Baba S, Nakamura M, Manago S, Suzuki A, et al. A single-strand conformation polymorphism method for the large-scale analysis of mutations/polymorphisms using capillary array electrophoresis. Electrophoresis 2002;23:2259–66.
24. Sasaki T, Tahira T, Suzuki A, Higasa K, Kukita Y, Baba S, et al. Precise estimation of allele frequencies of single-nucleotide polymorphisms by a quantitative SSCP analysis of pooled DNA. Am J Hum Genet 2001;68:214–8.
25. Yoshimoto K, Iwaki T, Inamura T, Fukui M, Tahira T, Hayashi K. Multiplexed analysis of post-PCR fluorescence-labeled microsatellite alleles and statistical evaluation of their imbalance in brain tumors. Jpn J Cancer Res 2002;93:284–90.
26. Rozen S, Skaletsky H. Primer3 on the WWW for general users and for biologist programmers. Methods Mol Biol 2000;132:365–86.
27. Baba S, Kukita Y, Higasa K, Tahira T, Hayashi K. Single-stranded conformational polymorphism analysis using automated capillary array electrophoresis apparatuses. Biotechniques 2003;34:746–50.
28. Higasa K, Kukita Y, Baba S, Hayashi K. Software for machine-independent quantitative interpretation of SSCP in capillary array electrophoresis (QUISCA). Biotechniques 2002;33:1342–8.
29. Mizoguchi M, Nutt CL, Mohapatra G, Louis DN. Genetic alterations of phosphoinositide 3-kinase subunit genes in human glioblastomas. Brain Pathol 2004;14:372–7.
30. Boehm D, Herold S, Kuechler A, Liehr T, Laccone F. Rapid detection of subtelomeric deletion/duplication by novel real-time quantitative PCR using SYBR-green dye. Hum Mutat 2004;23:368–78.
31. Girard L, Zochbauer-Muller S, Virmani AK, Gazdar AF, Minna JD. Genome-wide allelotyping of lung cancer identifies new regions of allelic loss, differences between small cell lung cancer and non-small cell lung cancer, and loci clustering. Cancer Res 2000;60:4894–906.
32. Buckley PG, Mantripragada KK, Benetkiewicz M, Tapia-Paez I, Diaz De Stahl T, Rosenquist M, et al. A full-coverage, high-resolution human chromosome 22 genomic microarray for clinical and research applications. Hum Mol Genet 2002;11:3221–9.
33. Mantripragada KK, Buckley PG, de Stahl TD, Dumanski JP. Genomic microarrays in the spotlight. Trends Genet 2004;20:87–94.
34. Schouten JP, McElgunn CJ, Waaijer R, Zwijnenburg D, Diepvens F, Pals G. Relative quantification of 40 nucleic acid sequences by multiplex ligation-dependent probe amplification. Nucleic Acids Res 2002;30:e57.
35. Rakha EA, Armour JA, Pinder SE, Paish CE, Ellis IO. High-resolution analysis of 16q22.1 in breast carcinoma using DNA amplifiable probes (multiplex amplifiable probe hybridization technique) and immunohistochemistry. Int J Cancer 2005;114:720–9.
36. Takata M, Suzuki T, Ansai S, Kimura T, Shirasaki F, Hatta N, et al. Genome profiling of melanocytic tumors using multiplex ligation-dependent probe amplification (MLPA): its usefulness as an adjunctive diagnostic tool for melanocytic tumors. J Dermatol Sci 2005;40:51–7.
37. Janne PA, Li C, Zhao X, Girard L, Chen TH, Minna J, et al. High-resolution single-nucleotide polymorphism array and clustering analysis of loss of heterozygosity in human lung cancer cell lines. Oncogene 2004;23:2716–26.
38. Hanahan D, Weinberg RA. The hallmarks of cancer. Cell 2000;100:57–70.
39. Devilee P, Cleton-Jansen AM, Cornelisse CJ. Ever since Knudson. Trends Genet 2001;17:569–73.
40. Ward JH. Hierarchical grouping to optimize an objective function. J Am Stat Assoc 1963;8:236–44.